

Probing the NMSSM via Higgs boson signatures from stop cascade decays at the LHC

Amit Chakraborty^a, Dilip Kumar Ghosh^b, Subhadeep Mondal^c,
 Sujoy Poddar^d, Dipan Sengupta^e

^a Department of Theoretical Physics, Tata Institute of Fundamental Research,
 1, Homi Bhabha Road, Mumbai-400 005, India.

^b Department of Theoretical Physics, Indian Association for the Cultivation of Science,
 2A & 2B, Raja S.C. Mullick Road, Jadavpur, Kolkata 700 032, India.

^c Harish-Chandra Research Institute, Chhatnag Road, Jhusi, Allahabad 211019, India.

^dNetaji Nagar Day College, 170/436 N.S.C. Bose Road, Kolkata 700092, India.

^e Laboratoire de Physique Subatomique et de Cosmologie, Universite Grenoble-Alpes, CNRS/IN2P3,
 53 Avenue des Martyrs, F-38026 Grenoble Cedex, France.

Abstract

Higgs signatures from the cascade decays of light stops are an interesting possibility in the next to minimal supersymmetric standard model (NMSSM). We investigate the potential reach of the light stop mass at the 13 TeV run of the LHC by means of five NMSSM benchmark points where this signature is dominant. These benchmark points are compatible with current Higgs coupling measurements, LHC constraints, dark matter relic density and direct detection constraints. We consider single and di-lepton search strategies, as well as the jet-substructure technique to reconstruct the Higgs bosons. We find that one can probe stop masses up to 1.2 TeV with 300 fb^{-1} luminosity via the di-lepton channel, while with the jet-substructure method, stop masses up to 1 TeV can be probed with 300 fb^{-1} luminosity. We also investigate the possibility of the appearance of multiple Higgs peaks over the background in the fat-jet mass distribution, and conclude that such a possibility is viable only at the high luminosity run of 13 TeV LHC.

1 Introduction

The discovery of a Higgs-like particle with mass close to 125 GeV by both the ATLAS [1] and CMS [2] collaborations has led us to a new crossroad. Measurements of its spin, CP quantum number and couplings to the standard model (SM) particles so far are consistent with SM predictions for the Higgs boson [3, 4]. The natural question is whether this Higgs-like particle is also one of the CP-even Higgs bosons of the supersymmetric (SUSY) models (for a review of supersymmetry, see Refs. [5–7]). The primary goal of the run-II of the LHC therefore is to look for new particles as well as investigate the properties and couplings of this Higgs boson more precisely.

In the minimal supersymmetric standard model (MSSM), in order to push the light CP-even Higgs boson mass up to 125 GeV, a sizeable amount of quantum correction is required. The dominant contribution comes from the light third generation squarks, namely the stops. However, to achieve a 125 GeV Higgs boson in the MSSM one requires to have maximally mixed or heavy stops (close to 1 TeV). This requirement, along with the lower limits imposed on the different SUSY particles (specially the gluino and the light stop) after the 8 TeV run at the LHC have pushed the fine-tuning problem of the SM to an uncomfortable level [8]. The next to minimal supersymmetric standard model (NMSSM) [9] provides a solution to this problem. The model extends the MSSM field content by the addition of a gauge singlet chiral superfield (\hat{S}). As a consequence of the coupling of this new gauge singlet superfield \hat{S} with the Higgs doublet superfields \hat{H}_u and \hat{H}_d , the $\lambda \hat{H}_u \hat{H}_d \hat{S}$ term in the NMSSM superpotential, the tree level Higgs boson mass receives an extra tree level

contribution which is proportional to the square of the singlet-doublet coupling λ . Therefore a relatively smaller radiative correction is required in the NMSSM to obtain a 125 GeV Higgs. This ensures that the fine-tuning issue is diluted to some extent in the NMSSM compared to the MSSM [10–15].

The phenomenology of the NMSSM is much richer than MSSM due to the presence of the additional superfield \hat{S} . The Higgs sector of the NMSSM consists of five neutral (three CP-even $H_{1,2,3}$ and two CP-odd $A_{1,2}$) and two charged (H^\pm) scalars. The neutral component of the scalar part of the gauge singlet superfield \hat{S} mixes with the neutral components of the Higgs fields, and thus there can be a significant doublet-singlet mixing after the Higgs mass matrix is diagonalized. For certain choices of the model parameters, one can find a light Higgs boson which is predominantly singlet like. Therefore regardless of the CP properties, its coupling with the SM gauge bosons will be highly suppressed. Therefore the constraints imposed by LEP cannot exclude such a singlet like light Higgs boson. Thus having additional Higgses in the vicinity of the SM-like 125 GeV Higgs boson is an attractive possibility in the NMSSM [16–21]. While the spin, parity and coupling measurements of the discovered Higgs boson indicate that it is the SM-like Higgs, it could very well be the second lightest CP-even Higgs boson of the NMSSM, with SM like couplings to fermions and gauge bosons.

The Higgs bosons in the NMSSM can arise from the cascade decays of stops and heavy neutralinos. A wide range of papers have studied the production of Higgs bosons and neutralino cascade decays to Higgs bosons in the NMSSM, and we refer some of them in [22–28]. The prospect of having additional NMSSM Higgs bosons in the vicinity of the 125 GeV Higgs boson was considered in [11], where the authors carefully analyzed the interplay of NMSSM Higgs bosons and the stop sector and concluded that one could achieve a modest level of fine tuning with a light stop below 1 TeV. Moreover, the possibility of the production of multiple Higgses in NMSSM was also considered in [29], where the authors considered pair production of SM like Higgs bosons from squark and gluino cascade decays.

In a R-parity conserved SUSY scenario, the lightest neutral, stable SUSY particle (LSP) serves as a good cold dark matter (DM) candidate. The presence of a singlet superfield in the NMSSM, that gives rise to an extra singlino component in the neutralino sector, results in a very interesting DM phenomenology. Moreover unlike the MSSM, a very light DM matter candidate as favored by some of the DM experiments [30, 31] can also be accommodated in NMSSM. Therefore a comprehensive phenomenological study of the interplay of the Higgs sector and the neutralino sector in the NMSSM is of prime importance at the LHC.

At this point it is pertinent to discuss some of the LHC analyses dedicated to stop searches at the 8 TeV run of LHC relevant to this study. Most of these searches by the ATLAS and CMS collaborations have been conducted in the framework of simplified topologies. The CMS collaboration has studied the prospect of discovering the light \tilde{t}_1 assuming 100% branching ratio (BR) for $\tilde{t}_1 \rightarrow t\chi_1^0$, and placed the limit on the stop mass up to 650 GeV for massless neutralinos in the single lepton + jets + \not{p}_T channel [32]. The decay of the heavier stop (\tilde{t}_2) to \tilde{t}_1 and the SM-like Higgs ($\tilde{t}_2 \rightarrow \tilde{t}_1 H_{\text{SM}}$) has also been studied by the CMS collaboration [33]. The limits at 8 TeV are rather weak, with the heavier stop up to 575 GeV and the lighter stop up to 400 GeV being ruled out with 19.5 fb^{-1} of integrated luminosity. Additionally, in the framework of gauge mediated supersymmetry breaking (GMSB), the channel $\tilde{t}_1 \rightarrow t\chi_1^0$, followed by the decay of χ_1^0 to H_{SM} and a Gravitino (\tilde{G}) was studied in [34]. The limits placed on the light stop mass for this particular scenario is about 400 GeV. Furthermore, the pair production of chargino and neutralino with the decay $\chi_2^0 \rightarrow \chi_1^0 H_{\text{SM}}$ has also been studied by the ATLAS collaboration, assuming degenerate masses for χ_1^\pm and χ_2^0 . The limit on $m_{\chi_2^0}$ was set to 250 GeV [35]. It has to be remembered that most of these experimental studies have been performed assuming that the branching ratios for all the topologies are 100%. A few phenomenological studies with boosted top and Higgs have also been performed for 14 TeV run of LHC in the simplified model scenarios and in the context of some specific models as well. In particular, the prospects of $\chi_1^\pm \chi_2^0 \rightarrow H_{\text{SM}} W \chi_1^0$ with boosted Higgs was studied in [36] in the context of the constrained minimal supersymmetric standard model (CMSSM). It was concluded that χ_1^\pm, χ_2^0 masses up to 400 GeV could be probed at 14 TeV LHC in this framework. The decay of heavier stops to $\tilde{t}_2 \rightarrow \tilde{t}_1 H_{\text{SM}}$ was considered in [37]. The author concluded that \tilde{t}_2 masses up to 1 TeV could be probed at 14 TeV with 100 fb^{-1} luminosity, in a simplified model scenario.

In this paper, we consider the production of Higgs bosons from the cascade decay of the \tilde{t}_1 in the NMSSM framework. We investigate the prospects of light stop pair production followed by the decay of \tilde{t}_1 to a top quark and any one of the heavier neutralinos ($\chi_{i=2,\dots,5}^0$), which subsequently decays to one of the neutral

Higgs states ($H_1, H_{\text{SM}} \equiv H_2, A_1$)¹ and the lightest neutralino, i.e., $\chi_i^0 \rightarrow \chi_1^0 + H_{1,\text{SM}}/A_1$. The produced Higgs in this case will be boosted if there is a significant mass gap between $m_{\chi_i^0}$ and $m_{\chi_1^0}$. Here we consider five benchmark points (BP) compatible with the current Higgs coupling measurements, DM relic density constraint, and direct detection constraints. The main characteristic feature of all these BPs is that the decay of the heavier neutralinos to the Higgses is dominant. We apply the jet substructure technique to reconstruct these boosted Higgs bosons to estimate the reach of stop searches in the context of 13 TeV run of LHC. We also analyze the possibility of the appearance of multiple Higgs peaks over the background in the fat-jet mass distribution. It is observed that the appearance of such peaks are only viable at very high luminosity run of LHC. However it is worth pursuing such a possibility to reveal the presence physics beyond the SM. We also compare our results with the generic lepton(s), jets + missing energy searches at the LHC.

The rest of the paper is organised as follows. In section 2 we discuss the choice of benchmark points, the relevant constraints imposed and briefly review some of the literature relevant to this study. In section 3, we discuss our collider analysis, while in section 4 we present our results and finally we conclude in section 5.

2 Benchmark points and constraints

As already discussed, we focus on the production of the Higgs bosons from the cascade decay of the \tilde{t}_1 . Thus we start with \tilde{t}_1 pair production followed by the cascade decay of the stop to neutralinos and Higgs. The final state therefore contains top quarks, Higgs bosons, and LSPs. The Higgs decays dominantly to pair of b-quarks, while we let the top quark decay inclusively. We present a sample Feynman diagram of the process of our interest in Fig. 1. Few representative cascade decay modes are shown below, where X collectively denotes the decay products of the top quarks and also other final state particles except the Higgses:

$$\begin{aligned}
 \text{pp} &\rightarrow \tilde{t}_1 \tilde{t}_1^* \rightarrow t \bar{t} \chi_2^0 \chi_2^0 \rightarrow t \bar{t} + 2H_{\text{SM}} + 2\chi_1^0 \rightarrow (b \bar{b})(b \bar{b}) + \not{p}_T + X \\
 \text{pp} &\rightarrow \tilde{t}_1 \tilde{t}_1^* \rightarrow t \bar{t} \chi_2^0 \chi_2^0 \rightarrow t \bar{t} + H_{\text{SM}} H_1 + 2\chi_1^0 \rightarrow (b \bar{b})(b \bar{b}) + \not{p}_T + X \\
 \text{pp} &\rightarrow \tilde{t}_1 \tilde{t}_1^* \rightarrow t \bar{t} \chi_2^0 \chi_3^0 \rightarrow t \bar{t} + H_{\text{SM}} H_1 + 2\chi_1^0 \rightarrow (b \bar{b})(b \bar{b}) + \not{p}_T + X \\
 \text{pp} &\rightarrow \tilde{t}_1 \tilde{t}_1^* \rightarrow t \bar{b} \chi_2^0 \chi_1^- \rightarrow t \bar{b} + W^- H_{\text{SM}}/H_1/H_3 + 2\chi_1^0 \rightarrow (b \bar{b}) + \not{p}_T + X.
 \end{aligned}$$

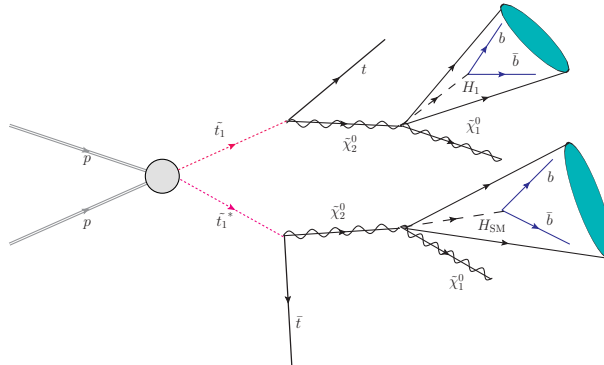


Figure 1: A sample Feynman diagram for the channel under consideration.

The decay of the next-to lightest supersymmetric particle (NLSP) to LSP + X ($X = Z/H_{\text{SM}}$) in the NMSSM framework has been already addressed in [38], where the authors pointed out that for a singlino like LSP satisfying DM constraints, this decay would lead to a reduction of missing transverse energy making it difficult to probe at the LHC. The authors also looked at the prospects of Higgs production from the cascade decay of squarks and noted that small values of λ and κ were required to satisfy the invisible Higgs decay

¹Throughout this paper we will denote the SM-like Higgs as $H_{\text{SM}} \equiv H_2$ and the rest of the Higgs spectrum contains H^\pm , $H_{1,3}$, $A_{1,2}$.

constraint by suppressing the mixing of the singlet like χ_1^0 with Higgsinos, for cases where $m_{\chi_1^0} \sim 5$ GeV. The authors showed that the $jjb\bar{b}$ background was significantly large at 13 TeV LHC and so they proposed that tagging multiple b-jets along with the requirement of a large number of jets can be useful to reduce the large background. The decay $\chi_{2,3}^0 \rightarrow \chi_1^0 H_{\text{SM}}$ was also discussed in [39], where the authors also argued along the same lines. The authors looked at $pp \rightarrow \chi_i^0 \chi_j^0 jj$, with subsequent decay of the neutralino states to the SM-like Higgs. They showed that four b-tagged jets in addition to \not{p}_T can be a viable channel at 14 TeV LHC. The authors also suggested ways of distinguishing MSSM from NMSSM by observing dark matter patterns and neutralino branching ratios at the colliders. This particular region of parameter space specific to the NMSSM has therefore received significant attention. From the above studies it is also evident that probing such a channel at the LHC environment is a very difficult task. A detailed collider study at 13 TeV LHC is preformed here.

The benchmark points for this study are chosen with the intention of probing the regions of parameter space where the decay of $\chi_{2,3}^0$ to LSP + Higgs is dominant. We present our five representative benchmark points in Table 1. The branching ratios of the relevant decay modes and some of the crucial observables corresponding to the benchmark points are tabulated in Table 2. The particle spectrum and decays are generated using NMSSMTOOLS-4.2.1 [40]. Since we are interested in the decay of the light stop, we decouple the rest of the spectrum, i.e, we set the mass of the gluino and the rest of the squarks and sleptons at 3 TeV. Furthermore, we want the light stop to be predominantly left handed and therefore we set the soft masses for the right handed 3rd generation squarks to be at 3 TeV, so that the decays $t_1 \rightarrow t \chi_{2,3}^0$ and $\tilde{t}_1 \rightarrow b \chi_1^{\pm}$ are dominant. It is pertinent to note that a detailed collider analysis for the left handed light stop was performed by some of the same authors in an earlier work using the boosted top technique in the context of phenomenological MSSM [41]. Since our primary channel of interest for the subsequent stage of the cascade is $\chi_{2,3}^0 \rightarrow \chi_1^0 H_{\text{SM}}/H_1/A_1$, we allow top to decay inclusively, while Higgs decays dominantly to $b\bar{b}$. It has to be remembered that the whole scenario is additionally complicated by the fact that one has to satisfy the DM relic density and also DM direct detection constraints, if χ_1^0 is assumed to be a valid DM candidate.

In order to ensure that $\chi_{2,3}^0$ has a large higgsino component, we fix M_1 and M_2 to 1.5 TeV for all benchmark points and vary μ_{eff} in the range of 260-280 GeV. This also ensures that $\chi_{4,5}^0$ are predominantly gaugino like and have mass close to 1.5 TeV. Thus they play no role in the cascade decay of the light stop. On the other hand, the large value of λ ensures that the lightest neutralino is predominantly singlino for all of the parameter space points. The two decay modes that compete here are $\chi_{2,3}^0 \rightarrow \chi_1^0 Z$ and $\chi_{2,3}^0 \rightarrow \chi_1^0 H_{1,\text{SM}}$, when the mass difference, $m_{\chi_{2,3}^0} - m_{\chi_1^0} > m_{H_{1,\text{SM}}}$ is satisfied. In the MSSM, this competition is predominantly determined by the gaugino-higgsino components of the neutralino, such that the decay of heavier neutralino states to lighter ones and Higgs has full gauge strength if one of the neutralino is gaugino like while the other is higgsino like. However, in the NMSSM, the LSP can have a significant amount of singlino admixture, and this is the case for our all the benchmark points. It is known that the Z boson only couples to the higgsino like component of the lightest neutralino and therefore the $\chi_1^0 \chi_2^0 Z$ coupling is suppressed for a dominantly singlino like neutralino. Hence $\chi_2^0 \rightarrow \chi_1^0 H_{\text{SM}}$ dominates in all our benchmark points (see Table 2). Here, we perform a small scan over the NMSSM parameter space and consider the parameters presented in Table 1 such that the relevant decay modes are dominant and all the present low energy constraints are satisfied. In the Higgs sector, we ensure that the LEP constraints as well as SM Higgs coupling constraints at the end of 8 TeV run of the LHC are satisfied [3, 4, 42]. The lightest Higgs boson being dominantly singlet like, the $H_1 ZZ$ coupling is suppressed ensuring that the LEP bounds are easily satisfied. A consequence of the singlet like H_1 is that the branching ratio of $\chi_{2,3}^0 \rightarrow \chi_1^0 H_1$ is rather small (see Table 2). We also note that M_A , the pseudoscalar mass parameter, plays an important role to satisfy the DM constraints. For the parameter space of our interest, the LSP annihilates dominantly via the pseudoscalar, and therefore a small tuning in the mass of M_A is required to obtain the DM relic density within 2σ of WMAP/PLANCK data [43, 44]. Additionally, we make sure that the benchmark points of our choice satisfies the direct detection cross-section bounds obtained from the LUX [45] collaboration.

All the benchmark points satisfy the following set of constraints:

- The mass of the SM-like Higgs must be within the range $123 \text{ GeV} < M_{H_{\text{SM}}} < 129 \text{ GeV}$. Due to the small difference in the central values of the ATLAS and CMS measurements and also considering the theoretical uncertainty in Higgs mass calculation, we use $126 \pm 3 \text{ GeV}$ as a conservative estimate [46, 47].
- The SM-like Higgs couplings to be within 2σ of the measured values provided by the ATLAS and CMS

	P1	P2	P3	P4	P5
$m_{\widetilde{Q}_3}$	830	920	1000	1180	1350
$\tan \beta$	10.2	12.2	10.4	10.3	10.2
λ	0.34	0.15	0.52	0.6	0.44
κ	0.06	0.03	0.09	0.09	0.07
A_λ	2700	2700	2700	2700	2700
A_κ	-1200	-1200	-1200	-1200	-1200
μ_{eff}	280	264	262	268	277
$m_{H_{SM}}$	124.3	124.9	124.3	125.1	124
m_{H_1}	67.1	67.1	62.3	73.8	67.2
m_{A_1}	214	226.8	194.4	154.0	193
$m_{\widetilde{t}_1}$	804.2	908.2	1003.7	1211	1392.5
$m_{\widetilde{b}_1}$	821.4	923.1	1018	1226	1408.6
$m_{\chi_1^0}$	98.6	107.2	87.3	77.6	87.4
$m_{\chi_2^0}$	290.1	268.0	282.7	293.2	292.4
$m_{\chi_3^0}$	293.5	273	283.1	294.2	295.1
$m_{\chi_1^\pm}$	284.7	268.5	266.5	273.2	282.5

Table 1: The parameters and masses for the five benchmark points. All the other parameters are set to their fixed values as described in the text. All masses are in GeV unit.

	P1	P2	P3	P4	P5
$\mu_{h_2}^{\gamma\gamma}(ggF), \mu_{h_2}^{\gamma\gamma}(VBF/VH)$	0.95, 0.96	0.94, 0.94	0.96, 0.96	0.92, 0.91	0.92, 0.91
$\mu_{h_2}^{\tau\tau}(ggF), \mu_{h_2}^{\tau\tau}(VBF/VH)$	1.0, 0.99	0.99, 0.97	0.99, 0.98	1.0, 1.0	1.0, 1.0
$\mu_{h_2}^{bb}(ttH), \mu_{h_2}^{bb}(VBF/VH)$	1.0, 0.97	0.95, 0.95	1.0, 1.0	1.01, 0.93	1.0, 1.0
$\Omega h^2, \sigma_{SI} (\times 10^{47}, \text{ cm}^2)$	0.123, 6.4	0.122, 1.9	0.115, 8.1	0.125, 1.8	0.126, 9.3
$\text{BR}(\widetilde{t}_1 \rightarrow t \chi_{2,3,4}^0)(\%)$	92	94	97	81	88
$\text{BR}(\widetilde{t}_1 \rightarrow b \chi_{1,2}^\pm)(\%)$	7	6	3	4	4
$\text{BR}(\chi_2^0 \rightarrow \chi_1^0 H_{1,\text{SM}})(\%)$	6, 60	8, 61	20, 57	18, 49	14, 54
$\text{BR}(\chi_3^0 \rightarrow \chi_1^0 H_{1,\text{SM}})(\%)$	3, 14	8, 1	3, 15	6, 16	4, 16.3
$\text{BR}(H_1 \rightarrow b\bar{b})(\%)$	86	69	91	90	85
$\text{BR}(H_2 \rightarrow b\bar{b})(\%)$	64	64	64	64	66
$\text{BR}(A_1 \rightarrow b\bar{b})(\%)$	1	1	1	90	1.5

Table 2: Some of the Higgs signal strengths, dark matter relic density, direct detection constraints and the relevant branching ratios for the particular study.

collaborations at the end of 7 + 8 TeV run of LHC with approx. 25 fb^{-1} of data [3,4](See Table 3 for more details.)

- The BR of the rare b-decays $B \rightarrow X_s \gamma$ and $B_s \rightarrow \mu^+ \mu^-$ are within 2σ of the experimental results [53]. We assume:

Channel	Signal Strength (μ)	
	CMS	ATLAS
$\gamma\gamma$	1.12 ± 0.24 [4]	1.17 ± 0.27 [48]
WW	0.83 ± 0.21 [4]	$1.09^{+0.23}_{-0.21}$ [49]
ZZ	1.0 ± 0.29 [4]	$1.44^{+0.40}_{-0.33}$ [50]
bb	0.84 ± 0.44 [4]	$0.52 \pm 0.32 \pm 0.24$ [51]
$\tau\tau$	0.91 ± 0.28 [4]	$1.43^{+0.43}_{-0.37}$ [52]

Table 3: Updated results on Higgs coupling measurements by the ATLAS and CMS collaborations at the end of 7 + 8 TeV run of the LHC with approx. 25 fb^{-1} of data.

$$2.77 \times 10^{-4} < \text{BR}(B \rightarrow X_s \gamma) < 4.09 \times 10^{-4}$$

$$1.0 \times 10^{-9} < \text{BR}(B_s \rightarrow \mu^+ \mu^-) < 5.2 \times 10^{-9}$$

- The LEP lower bound on the chargino mass, $M_{\chi_1^\pm} > 103.5 \text{ GeV}$ [42].
- We apply the upper bounds on the DM direct detection cross-section from LUX [45] and allow the DM relic density to be within 2σ of the WMAP/PLANCK [43, 44] data. Note that, precise value of DM relic density do not have any significant impact on our final results. We assume,

$$0.115 \leq \Omega_{\text{DM}} h^2 \leq 0.126.$$

Before we end this section, we would like to remind the readers that for all our benchmark points, the branching ratios for the decay $\tilde{t}_1 \rightarrow t \chi_{2,3}^0$ are significantly large owing to the large higgsino component in $\chi_{2,3}^0$ (see Table 2). The dominantly Higgsino-like χ_2^0 and largely singlino-like χ_1^0 ensure that $\chi_2^0 \rightarrow \chi_1^0 H_{\text{SM}}$ is significantly large, which is necessary for our collider strategy. Since H_{SM} is SM-like, it has a large branching ratio to $b\bar{b}$, while H_1 , due to the large singlet component and reduced coupling to ZZ also dominantly decays to $b\bar{b}$. From Table 2, it is evident that all the reduced signal strengths of the SM-like Higgs are well within 2σ of the limits imposed from the Higgs coupling measurements at the LHC. With these comments on the benchmark points, we now proceed to discuss our signal and background collider analysis in the next section.

3 Analysis of the signal and background

In this section we describe the strategy for the collider study. The entire analysis is divided into two parts: first we use the jet substructure technique to analyze the boosted Higgs scenario. This is followed by the standard leptonic search strategies at the LHC. We then compare these two methods and discuss the merits and demerits of each of these two procedures.

3.1 Jet substructure analysis

The Higgs tagging technique, introduced in the work of Butterworth-Davison-Rubin-Salam (BDRS) [54], has emerged as a powerful tool to study physics in the boosted regime. The efficacy of the BDRS tagger lies in the sharp resolution of the Higgs peak in the $H \rightarrow b\bar{b}$ channel. In the analysis, we apply the BDRS Higgs tagger to tag the Higgs originating from the decay of the heavier neutralinos. From Table 1, it is clear that the mass difference $m_{\chi_2^0} - m_{\chi_1^0}$ is not significantly big enough to generate a large boost to the Higgs. However, being part of a cascade decay, the boost to the Higgs boson originate from the two step decay chain of the stop. To demonstrate the larger boost in the signal process as compared to the background,

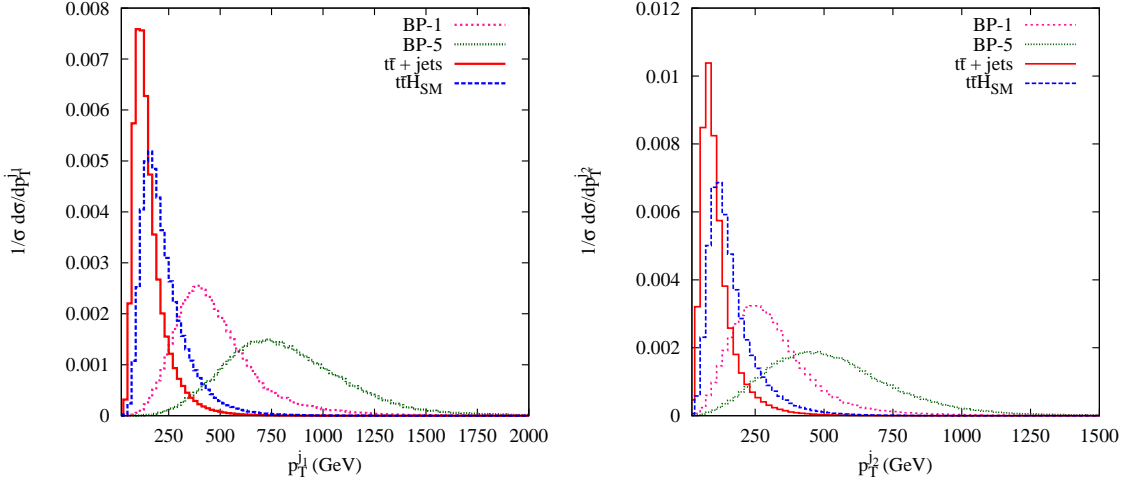


Figure 2: p_T -distribution of the leading two fat-jets for 13 TeV at the LHC. We reconstruct the jets using the C/A algorithm with jet radius $R = 1.2$. The benchmark points BP1 and BP5 are as tabulated in Table 2.

we present, in Fig. 2, the p_T distribution of the leading two “fat-jets” reconstructed using the Cambridge-Aachen (C/A) [55] jet algorithm with the jet radius $R=1.2$, for two benchmark points BP1 and BP5, as well as the SM $t\bar{t} + \text{jets}$ background. One can observe that for the signal, the peak of the distribution is over 400 GeV, while the background falls sharply from 200 GeV. We notice that with the increase in the stop mass (BP1 to BP5), the fat-jet distribution moves to the higher p_T region, as expected. To optimize the Higgs tagging efficiency we considered the values of the fat-jet radius R to be 1, 1.2 and 1.5 and concluded that $R=1.2$ is the best choice in terms of signal to background ratio. Furthermore we varied the jet p_T threshold, considering three different values 200 GeV, 400 GeV, 600 GeV and arrived at the conclusion that a jet radius $R=1.2$ and a jet p_T threshold of 200 GeV gives the best efficiency in terms of enhancement in the signal and reduction of background. Since the boost to the Higgs boson in our case is not significantly large, we achieve a modest Higgs tagging efficiency ($\epsilon \sim 5\text{-}6\%$ for $p_T \sim 200\text{-}300$ GeV). However this is an order of magnitude larger compared to the largest background in terms of cross section, namely $t\bar{t} + \text{jets}$ (see Table 4 and 5). An added advantage of using the BDRS Higgs tagger is that it uses a filtering technique to discard the contamination from the underlying events, which in turn helps to improve the resolution of the Higgs peak. As a consequence of the superior mass resolution, it is also a powerful tool against the backgrounds containing multiple b-jets like $t\bar{t} + \text{jets}$, $Z(\rightarrow b\bar{b}) + \text{jets}$, $t\bar{t}b\bar{b}$, $t\bar{t}W$, $t\bar{t}Z$. The SM backgrounds that we consider are listed below,

- $t\bar{t} + \text{jets}$: The decay of top quark yield two b-jets in the final state and thus the reconstructed fat-jet could in principle fake a Higgs signal.
- $Z(\rightarrow b\bar{b}) + \text{jets}$: In this case although the fat-jet mass distribution should peak at the Z boson mass there might be a large tail. Owing to the large $Z + \text{jets}$ cross section, this could potentially be significant in the end.
- $t\bar{t}b\bar{b}$, $t\bar{t}Z$, $t\bar{t}W$: These backgrounds contain at least 2 b-jets, which may be tagged as a fake SM Higgs boson.
- $t\bar{t}H_{\text{SM}}$: This constitutes the irreducible background to our signal with at least one tagged Higgs jet

and \not{p}_T . However the Higgs in this case is not expected to be as boosted as the signal.

We use NMSSMTOOLS-4.2.1 [40, 56–58] to generate the NMSSM mass spectrum, while signal and background events are simulated using MADGRAPH5 [59] and passed to PYTHIA6 (version 6.4.26) [60] for showering and hadronization. For the signal ($\tilde{t}_1 \tilde{t}_1^* + 2$ jets) and $t\bar{t}/Z/W +$ jets (up to 2 jets), we perform the matrix element parton shower (ME-PS) merging using the MLM prescription [61] with a merging parameter of 30 GeV. We use FastJet-3.1.0 [62] for jet reconstruction, and implementation of our jet substructure analysis. The rare b-decay observables, DM relic density and direct detection cross-sections are calculated using NMSSMTOOLS.

We observe that even after tagging of the Higgs jet, there is still a significant amount of hadronic activity in the signal process. This activity can be used as an effective handle against the background. Therefore the jet reconstruction procedure in our case is a two step process. We first reconstruct fat-jets using the Cambridge-Aachen (C/A) [55] algorithm using a jet radius of $R=1.2$ with a jet p_T threshold of 200 GeV followed by the use of the BDRS [54] Higgs tagger with a default mass drop criteria of $\mu = 0.67$ and the filtering parameter $R_{\text{filt}} = \min(R_{b\bar{b}}/2, 0.3)$. Once one (or multiple) SM-like Higgs boson(s) are tagged, we remove those particles from the fat-jet list and recluster the remaining stable hadrons using anti- k_T [63] jet algorithm with a jet radius of $R=0.4$, $p_T \geq 20$ GeV. We select jets with $p_T^j \geq 30$ GeV and pseudorapidity $|\eta_j| < 3$ for further collider analysis. Leptons (electrons and muons) are selected with $p_T^\ell > 10$ GeV and $|\eta_\ell| < 2.5$. Isolation of leptons are performed by demanding that the sum of the scalar p_T of all stable visible particles within a cone of radius $\Delta R = 0.2$ around the lepton should not exceed 10% (15% for muons) of p_T^e (p_T^μ). The missing transverse energy is constructed using all the stable final state visible particles with all jets with $p_T^j > 20$ GeV and $|\eta_j| < 4.5$, and all leptons with $p_T^\ell > 10$ GeV and $|\eta_\ell| < 2.5$. Following the ATLAS collaborations [64], we consider a p_T -dependent b-tagging efficiency :

$$\eta_b = \begin{cases} 0 & \text{for } p_T^b \leq 20 \text{ GeV} \\ 0.6 & \text{for } 20 \text{ GeV} < p_T^b < 50 \text{ GeV} \\ 0.75 & \text{for } 50 \text{ GeV} < p_T^b < 400 \text{ GeV} \\ 0.5 & \text{for } p_T \geq 400 \text{ GeV} \end{cases}$$

After generating events, the following set of kinematic cuts are applied,

- C1: We demand that at least one of the fat-jets is identified as the SM-like Higgs boson with the criteria $110 \text{ GeV} < m_J < 140 \text{ GeV}$, where m_J denotes the fat-jet mass. The fat-jet is deemed to be a Higgs-like jet if and only if two b-jets are identified inside the fat-jet. In the signal process, however, there are additional Higgs bosons which can be tagged and therefore at the end of all selection cuts we look at the m_J distribution, to find if additional peaks are visible over the background. The Higgs boson tagging ensures that most of the backgrounds with multiple b-jets in the final state are significantly reduced.
- C2: In this work we consider a hadronic final state, and therefore we impose a lepton veto.
- C3: For the signal, even after at least one SM-like Higgs boson is tagged, there are significant number of b-jets originating from the top quarks. However, these extra b-jets are unlikely to be present in the backgrounds like $Z (\rightarrow b\bar{b}) +$ jets, $t\bar{t} +$ jets after satisfying the Higgs mass criteria. Therefore, we demand at least one additional b-jet in the event.
- C4: An additional selection criteria of $H_T = \sum_j p_T^j > 800$ GeV is imposed. The jets in this case are the anti- k_T jets constructed by reclustering the rest of the hadronic sample after removing the hadrons contributing to the Higgs tagged jet as mentioned earlier. The larger hadronic activity in the signal implies a larger value of H_T compared to the background. This cut is particularly useful in suppressing the irreducible $t\bar{t}H_{\text{SM}}$ background. In the left panel of Fig. 3, we present the H_T distribution corresponding to two signal benchmark points BP1 and BP5, along with the two dominant backgrounds $t\bar{t} +$ jets and $t\bar{t}H_{\text{SM}}$.
- C5: As a final selection criteria we impose a \not{p}_T cut of 175 GeV. The signal \not{p}_T distribution is harder compared to that of the SM backgrounds because of the heavy LSP in the final state of the signal

events. In the right panel of Fig. 3, the \not{p}_T distribution for the signal and $t\bar{t} + \text{jets}$ are presented to illustrate this feature.

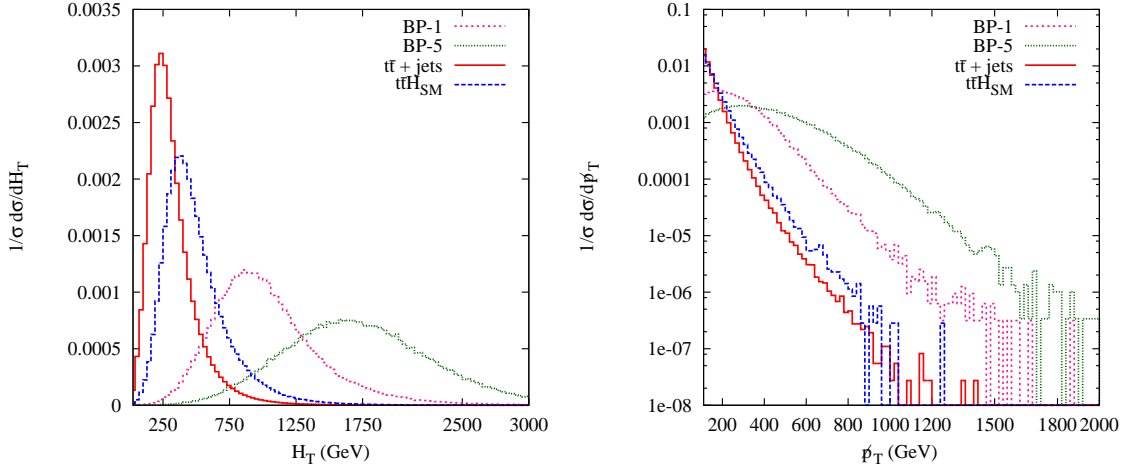


Figure 3: Left panel shows the distribution of H_T where $H_T = \sum_j p_T^j$ with the anti- k_T jets selected after imposing the basic Higgs tagging criteria, while right panel displays the distribution of the \not{p}_T at the 13 TeV LHC.

3.2 Alternative analysis: Final state with leptons

In order to understand whether the jet substructure technique is more effective than other search strategies, we perform a separate collider analysis with leptonic final states. Here we probe two such possible scenarios, one dedicated to the single lepton final state (denoted as Case-I), while other being the di-leptonic channel (denoted as Case-II). The SM backgrounds for both these channels are $t\bar{t} + \text{jets}$, $W(\rightarrow l\nu) + \text{jets}$, $Z + \text{jets}$, $t\bar{t}Z(\rightarrow \ell^+\ell^-)$, $t\bar{t}W$ (where the leptons can originate either from W or from the top) and the irreducible $t\bar{t}H_{\text{SM}}$. To analyze these two channels, we devise two sets of search strategies and optimize our selection cuts to obtain a good signal significance at the LHC. We use FASTJET to reconstruct the jets with anti- k_T [63] jet algorithm with a jet radius of $R=0.4$ and $p_T^{\min} \geq 20$ GeV. We select jets with $p_T^j \geq 30$ GeV and $|\eta_j| \leq 3$ for further analysis. Below, we list the optimized selection cuts for both the cases separately.

1. Case I (Single lepton) :

- C6: We demand at least 4 jets with $p_T^{j1} > 200$ GeV, $p_T^{j2} > 150$ GeV, $p_T^{j3} > 100$ GeV, $p_T^{j4} > 50$ GeV, since the signal has a significantly larger number of hard jets as compared to the background.
- C7: Additionally, we demand at least 2 b-tagged jets, to suppress backgrounds like $W(\rightarrow l\nu) + \text{jets}$.
- C8: A single isolated lepton is required with $p_T^\ell \geq 20$ GeV and $|\eta_\ell| \leq 2.5$.
- C9 : Since the leptonic mode is under investigation, a large \not{p}_T is required to suppress backgrounds like $t\bar{t} + \text{jets}$, $t\bar{t}H_{\text{SM}}$. Therefore a $\not{p}_T > 400$ GeV is imposed.
- C10 : Due to the significantly larger jet activity in the signal, we impose $H_T = \sum p_T^j > 600$ GeV, where jets satisfying the basic selection criteria are considered here.

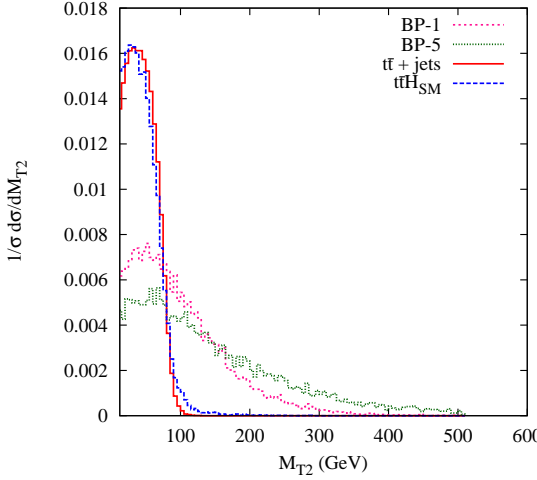


Figure 4: The M_{T2} distribution at 13 TeV LHC energy for the benchmark points P1, P5 and the SM backgrounds $t\bar{t}H_{SM}$ and $t\bar{t} + \text{jets}$.

- C11 : The SM process $t\bar{t}H_{SM}$, with one of the tops decaying leptonically is the largest background. To suppress this, we demand that the transverse mass of the lepton and missing transverse energy of the system, $M_T(\ell, \not{p}_T) = \sqrt{2p_T^\ell \times \not{p}_T \times (1 - \cos \phi(\ell, \not{p}_T))} > 200$ GeV. This ensures that the single lepton final states originating from the W boson are suppressed as the end point of the $M_T(\ell, \not{p}_T)$ distribution is expected to be bounded from above by the mass of the W boson. However, for the signal the presence of the additional χ_1^0 ensures that the end point of the $M_T(\ell, \not{p}_T)$ distribution is shifted beyond the W boson mass.
- C12: Events with number of jets greater than six are accepted.

2. **Case II (Di-lepton)** The di-lepton channel, although being cleaner compared to the single lepton channel, has the disadvantage of a lower signal cross section. We optimize the di-lepton channel by imposing the following set of cuts.

- C13 : We demand at least 3 jets with $p_T^{j1} > 150$ GeV, $p_T^{j2} > 100$ GeV, $p_T^{j3} > 50$ GeV.
- C14 : At least two b-tagged jets are required.
- C15 : We demand two isolated leptons with $p_T^\ell > 20$ GeV and $|\eta_\ell| < 2.5$.
- C16 : In order to suppress the backgrounds like $t\bar{t} + \text{jets}$, $t\bar{t}H_{SM}$, which yield di-leptons from the W decay, we use the variable M_{T2} [65, 66], defined as,

$$M_{T2}(\vec{p}_T^{\ell 1}, \vec{p}_T^{\ell 2}, \vec{\not{p}}_T) = \min_{\vec{\not{p}}_T = \vec{p}_T^{\ell 1} + \vec{p}_T^{\ell 2}} \left[\max\{M_T(\vec{p}_T^{\ell 1}, \vec{\not{p}}_T^1), M_T(\vec{p}_T^{\ell 2}, \vec{\not{p}}_T^2)\} \right], \quad (1)$$

where $\ell 1$ and $\ell 2$ are the two isolated leptons, $\vec{\not{p}}_T$ is the total missing transverse momentum of the event and $M_T(\vec{p}_T^{\ell 1}, \vec{p}_T^{\ell 2})$ is the transverse mass of the system, defined as

$$M_T(\vec{p}_T^{\ell 1}, \vec{p}_T^{\ell 2}) = \sqrt{2|\vec{p}_T^{\ell 1}| |\vec{p}_T^{\ell 2}| (1 - \cos \phi)},$$

ϕ being the (azimuthal) angle between $\vec{p}_T^{v_1}$ and $\vec{p}_T^{v_2}$. In the definition of Eq.1, \vec{p}_T^1 and \vec{p}_T^2 are the two hypothetical splits of the total missing transverse momentum. It is assumed that the mass of the invisible particles are zero [67]. The use of di-leptonic M_{T2} to suppress SM backgrounds has been considered previously in a host of other works, for example see Refs. [41, 68–70]. For leptons originating from the decay of the top quark, the value of M_{T2} is bounded by the W mass, whereas for signal the presence of χ_1^0 ensures that the distribution is shifted beyond the W mass. The signal and background distribution illustrating this feature is presented in Fig. 4. In this work, we set $M_{T2} > 150$ GeV.

- C17: Additionally we impose a criteria on the total missing transverse momentum, $\cancel{p}_T > 400$ GeV.

4 Results

In this section, we summarize our findings based on the collider simulation described in the previous section. We begin our discussion with the jet substructure analysis. The event summary for the signal after individual selection cuts are presented in Table 4, while in Table 5 the event summary for the backgrounds are tabulated. The second column of Table 4 corresponds to the NLO pair production cross-section of the light stop, as obtained from the official LHC supersymmetry cross section working group [71], corresponding to the benchmark points in Table 2. The cross sections for $t\bar{t} + \text{jets}$ are obtained using Madgraph5 with an appropriate K-factor for 13 TeV LHC, while for the cross section of $t\bar{t}H_{\text{SM}}$ process we use LHC Higgs cross-section working group report [72]. Although all the other backgrounds like $W/Z + \text{jets}$, $t\bar{t}b\bar{b}$, $t\bar{t}Z$, $t\bar{t}W$ as mentioned in the previous section were simulated, we present only $t\bar{t} + \text{jets}$ and $t\bar{t}H_{\text{SM}}$, as these are the dominant ones. It was checked that the choices of the selection cuts are such that other processes do not contribute to the final background cross section.

		Effective cross-section after the cuts (in fb)				
Signal	Production c.s. (fb)	C1	C2	C3	C4	C5
P1	27.2	1.18	0.58	0.48	0.25	0.146
P2	12	0.42	0.21	0.17	0.11	0.0794
P3	6	0.22	0.11	0.09	0.07	0.0529
P4	1.5	0.0497	0.0262	0.0225	0.0193	0.0161
P5	0.5	0.0258	0.0139	0.0121	0.0115	0.0096

Table 4: **Jet Substructure:** Event summary for the signal after individual cuts as described in the text. The simulation is performed at 13 TeV LHC energy. From 3rd column, we show the effective cross-section (c.s.) after all the event selection cuts have been applied.

From the 3rd column to the 7th column (C1-C5), we present the cut flow, normalized to the cross sections after imposing the selection cuts, as discussed in the previous section. Similarly, in Table 5, we discuss the event summary for the backgrounds after each cut. As can be observed from the 3rd column of Table 4, about 3-6% percent of the events have at least one tagged Higgs for the signal events. The $t\bar{t} + \text{jets}$ background is reduced by 99.89% (see Table 5, 3rd column) while backgrounds like $W/Z + \text{jets}$, $t\bar{t}b\bar{b}$, $t\bar{t}Z$, $t\bar{t}W$ (not shown in the Table) are reduced to negligible amounts. The largest background, as expected is $t\bar{t}H_{\text{SM}}$, with a tagging efficiency of about 2.8%. Therefore to reduce this background the subsequent cuts C2-C5 play an important role. From Table 5, we notice that the principal cut to suppress the rest of the $t\bar{t} + \text{jets}$ background is the demand of extra b-jets (cut C3) after satisfying the criteria of at least one SM-like Higgs. As mentioned earlier, these extra b-jets are unlikely to be present in the background and we observe that about 98% of the remaining $t\bar{t} + \text{jets}$ background is further rejected. In signal and $t\bar{t}H_{\text{SM}}$ however these extra b-jets are naturally present, and therefore they are not significantly suppressed. To suppress the $t\bar{t}H_{\text{SM}}$ background, we employ the cut on H_T and \cancel{p}_T as noted in the previous section. Even after the Higgs tag the presence of significantly high energetic jets from the stop decay as compared to $t\bar{t}H_{\text{SM}}$ and $t\bar{t} + \text{jets}$ ensures

		Effective cross-section after the cuts (in fb)				
SM bkg	Production c.s. (fb)	C1	C2	C3	C4	C5
t̄t+ jets	700000	751.02	554.85	7.5	0	0
ttH _{SM}	500	14.45	9.76	7.47	0.5	0.028
Total bkg						0.028

Table 5: **Jet Substructure:** Event summary for the backgrounds (bkg) after individual cuts as described in the text. Numbers in the last column show the final cross-section (c.s.) after all the event selection cuts are applied. For the t̄t+ jets background, we generate a matched sample of t̄t+ 0 jet, t̄t+ 1 jet and t̄t+ 2 jets using Madgraph. We also consider W+jets and Z+jets backgrounds, however both of them are identically zero at the end of C5.

	m _{t̄t} (GeV)	Signal(N _S) (Background(N _B))			Significance(\mathcal{S}) for $\kappa = 10\%$		
		100 fb ⁻¹	300 fb ⁻¹	1000 fb ⁻¹	100 fb ⁻¹	300 fb ⁻¹	1000 fb ⁻¹
P1	804.3	14.6 (2.8)	43.8 (8.4)	146 (28)	8.6	14.5	24.37
P2	908.2	7.94 (2.8)	23.82 (8.4)	79.4 (28)	2.75	7.9	13.25
P3	1003.7	5.29 (2.8)	15.87 (8.4)	52.9 (28)	1.83	5.25	8.83
P4	1211.5	1.61 (2.8)	4.83 (8.4)	16.1 (28)	0.55	1.6	2.69
P5	1392.5	0.96 (2.8)	2.88 (8.4)	9.6 (28)	0.33	0.95	1.6

Table 6: **Jet Substructure:** The summary of our signal and backgrounds. Columns 3-5 show the number of signal (total background) events for three values of the integrated luminosity: 100 fb⁻¹, 300 fb⁻¹ and 1000 fb⁻¹ at 13 TeV LHC. The columns 6-8 show the statistical significance of our signal for the above three integrated luminosities. For each value of the integrated luminosity the significances are shown considering $\kappa = 10\%$ systematic uncertainty.

that the H_T distribution is extended well beyond 1 TeV. The optimized H_T cut of 800 GeV kills the ttH_{SM} background by about 93%, while the t̄t + jets background is entirely wiped out. After all cuts, the only surviving background turns out to be ttH_{SM} as expected, with the background cross section being 0.028 fb.

The cut efficiency after all the selection cuts, in the jet substructure scenario, increases steadily from the benchmark points P1 to P5 due to a slight increase in the Higgs tagging efficiency as well as an increase in the strength of H_T and p_T cuts. However the rapid fall of the stop pair production cross-section with increasing mass results in a minuscule final cross-section for stop masses above 1 TeV. To project the reach at 13 TeV, we define the signal significance (\mathcal{S}) as $S/\sqrt{(B + (\kappa B)^2)}$, where we include a systematic uncertainty factor of κ in the background estimation to compensate for the fact that we do not perform any dedicated detector simulation in this study. For this study we choose κ to be 10%. In Table 6, the signal significances for 100, 300, 1000 fb⁻¹ of integrated luminosity are tabulated in columns 6-8 for the five benchmark points. It can be noted that one can probe a light stop mass up to 800 GeV (P1) at 100 fb⁻¹ integrated luminosity at 13 TeV LHC with a significance > 5 , while stop masses up to 1 TeV (P3) can be observed at 300 fb⁻¹ luminosity. The signal suffers because of low production cross section, and only with the very high luminosity run at LHC (i.e 3000 fb⁻¹), one can achieve signal significances greater than 5 σ for the benchmark points P4 and P5 with stop masses greater than 1 TeV. We also observe that one could exclude m_{t̄t} \sim 1.2 TeV for 300 fb⁻¹ integrated luminosity with the jet substructure technique.

We compare the results obtained using the jet substructure method with the leptonic searches for this channel. We first analyze the case of single lepton as denoted by Case-I in the previous section. In Table 7 and Table 8, we summarize the event yields (normalized to cross section) for the signal and backgrounds

		Effective cross-section after the cuts (in fb)						
Signal	Production c.s. (fb)	C6	C7	C8	C9	C10	C11	C12
P1	27.2	16.39	10.44	3.55	0.442	0.441	0.27	0.239
P2	12	8.49	5.5	1.88	0.315	0.314	0.2	0.176
P3	6	4.34	2.54	0.88	0.259	0.259	0.169	0.139
P4	1.5	1.17	0.74	0.246	0.109	0.109	0.077	0.061
P5	0.5	0.45	0.29	0.098	0.040	0.040	0.028	0.0255

Table 7: **One lepton**: Event summary for the signal after individual cuts as described in the text. In the last column we show the final cross-section (c.s.) after all the event selection cuts have been applied.

		Effective cross-section after the cuts (in fb)						
SM bkg	Production c.s. (fb)	C6	C7	C8	C9	C10	C11	C12
t̄t+ jets	700000	20465.1	8130.2	1410.6	9.13	8.96	5.6	2.28
ttH _{SM}	500	54.75	37.12	8.1	0.089	0.089	0.054	0.036
W + jets	83315178	6153.2	0	0	0	0	0	0
Z + jets	42070505	4115.1	470.3	0	0	0	0	0
Total bkg								2.316

Table 8: **One lepton**: Event summary for the backgrounds (bkg) after individual cuts as described in the text. In the last column we show the final cross-section (c.s.) after all the event selection cuts have been applied. For the t̄t+ jets background we have generated a matched sample of t̄t+ 0 jet, t̄t+ 1 jet and t̄t+ 2 jets using Madgraph.

		Signal(N _S) (Background(N _B))			Significance(\mathcal{S}) for $\kappa = 10\%$		
	m _{tilde t₁} (GeV)	100 fb ⁻¹	300 fb ⁻¹	1000 fb ⁻¹	100 fb ⁻¹	300 fb ⁻¹	1000 fb ⁻¹
P1	804.3	23.9 (231.6)	71.7 (694.8)	239 (2316)	0.86	0.96	1.01
P2	908.2	17.6 (231.6)	52.8 (694.8)	176 (2316)	0.64	0.71	0.74
P3	1003.7	13.9 (231.6)	41.7 (694.8)	139 (2316)	0.51	0.56	0.58
P4	1211.5	6.1 (231.6)	18.3 (694.8)	61 (2316)	0.22	0.25	0.26
P5	1392.5	2.55 (231.6)	7.65 (694.8)	25.5 (2316)	0.09	0.10	0.11

Table 9: **One lepton**: The summary of our signal and backgrounds. Columns 3-5 show the number of signal (total background) events for three values of the integrated luminosity: 100 fb⁻¹, 300 fb⁻¹ and 1000 fb⁻¹. The columns 6-8 show the statistical significance of our signal for the above three integrated luminosities. For each value of the integrated luminosity the significance is shown for three choices of the amount of possible systematic uncertainties, $\kappa = 10\%$.

respectively. We find that the W+ jets background is entirely killed by the demand of b-tagged jets, as expected. For the Z + jets background, the demand of two b-tagged jets, along with four hard jets implies that no isolated lepton is expected to be present. Therefore, imposition of the single lepton criteria (see column C8, Table 8) eliminates the Z+ jets background. The remaining background consists of t̄t + jets

and $t\bar{t}H_{SM}$. As can be seen from column 9 in Table 8, \not{p}_T along with H_T and M_T suppresses this set to a negligible level. However the small starting cross section for the signal essentially leads to the fact that the signal significance is not large enough for a discovery (or an exclusion) even at the 13 TeV high luminosity scenario for these benchmark points as can be observed from Table 9.

We next turn our attention to the di-lepton channel, denoted by case-II in the previous section. The signal and background yields in this case are tabulated in Table 10 and Table 11 respectively corresponding to the selection cuts C13 - C17 described in the last section. The demand for two isolated leptons in cut C13 suppresses the $W +$ jets background, while rest of the background is suppressed by the M_{T2} cut (C16). The M_{T2} cut is expected to be bounded from above by the mass of the W boson for the background, while for signal it is expected to extend to higher values due to the presence of large missing energy. We observe that the backgrounds like $t\bar{t} +$ jets is reduced to zero (0) after the M_{T2} cut, while there is a small residue from the $t\bar{t}H_{SM}$ background, which are further reduced by the \not{p}_T cut of C17. In Table 12, we observe that for the di-lepton channel, up to 1 TeV stops can be discovered with 100 fb^{-1} integrated luminosity, while a light stop mass up to 1.2 TeV can be discovered with 300 fb^{-1} of luminosity. Therefore we conclude that the di-lepton channel is most suited to probe the heavier \tilde{t}_1 mass with the benchmark points depicted in Table 2. We also observe that stop masses up to 1.4 TeV can be excluded at 13 TeV LHC, with 300 fb^{-1} luminosity.

		Effective cross-section after the cuts (in fb)				
Signal	Production c.s. (fb)	C13	C14	C15	C16	C17
P1	27.2	24.61	15.29	1.49	0.17	0.038
P2	12	11.31	7.17	0.63	0.096	0.0264
P3	6	5.65	3.19	0.297	0.061	0.0262
P4	1.5	1.43	0.875	0.065	0.019	0.012
P5	0.5	0.494	0.314	0.026	0.0069	0.0035

Table 10: **Two lepton:** Event summary for the signal after individual cuts as described in the text. In the last column we show the final cross-section (c.s.) after all the event selection cuts have been applied.

		Effective cross-section after the cuts (in fb)				
SM bkg	Production c.s. (fb)	C13	C14	C15	C16	C17
$t\bar{t} +$ jets	700000	105014.18	38630.79	515.89	0	0
$t\bar{t}H_{SM}$	500	179.56	116.06	3.01	0.007	0.001
$W +$ jets	83315178	123064.92	0	0	0	0
$Z +$ jets	42070505	78891.62	4799	0	0	0
Total bkg						0.001

Table 11: **Two lepton:** Event summary for the backgrounds (bkg) after individual cuts as described in the text. In the last column we show the final cross-section (c.s.) after all the event selection cuts have been applied. For the $t\bar{t} +$ jets background we have generated a matched sample of $t\bar{t} + 0$ jet, $t\bar{t} + 1$ jet and $t\bar{t} + 2$ jets using Madgraph.

Finally, we examine the possibility of the detection of multiple Higgs peaks in the fat-jet mass (m_J) distribution over the SM background, where J denotes the fat-jet. In Fig. 5, we plot the fat-jet distribution for the jet substructure technique at 300 , 1000 , and 3000 fb^{-1} luminosity respectively. We plot first six

	$m_{\tilde{t}_1}$ (GeV)	Signal(N_S) (Background(N_B))			Significance(\mathcal{S}) for $\kappa = 10\%$		
		100 fb^{-1}	300 fb^{-1}	1000 fb^{-1}	100 fb^{-1}	300 fb^{-1}	1000 fb^{-1}
P1	804.3	3.8 (0.1)	11.4 (0.3)	38 (1)	12.1	20.8	37.8
P2	908.2	2.64 (0.1)	7.92 (0.3)	26.4 (1)	8.34	14.4	26.3
P3	1003.7	2.62 (0.1)	7.86 (0.3)	26.2 (1)	8.28	14.3	26.0
P4	1211.5	1.2 (0.1)	3.6 (0.3)	12.0 (1)	3.79	6.56	11.9
P5	1392.5	0.35 (0.1)	1.1 (0.3)	3.5 (1)	1.1	2.0	3.48

Table 12: **Two lepton**: The summary of our signal and backgrounds. Columns 3-5 show the number of signal (total background) events for three values of the integrated luminosity: 100 fb^{-1} , 300 fb^{-1} and 1000 fb^{-1} . The columns 6-8 show the statistical significance of our signal for the above three integrated luminosities. For each value of the integrated luminosity the significance is shown for three choices of the amount of possible systematic uncertainties, $\kappa = 10\%$.

PT-ordered fat-jet masses at the end of our selection cut (C5) in our jet substructure Higgs analysis. In these plots we demand two b-tagged jets only for the fat-jet satisfying the 125 GeV Higgs criteria, i.e, $110 < m_j < 140$ GeV. We observe that while the SM Higgs peak is overwhelmingly visible at all the luminosity options, one can also observe slight excesses in three different masses over the $t\bar{t}H_{\text{SM}}$ background. We find small excesses in the lighter CP even Higgs boson (~ 65 GeV), Z boson (~ 91 GeV) as well as at the top quark (~ 172 GeV) masses. With a better branching ratio of $\chi_i^0 \rightarrow \chi_1^0 H_1$ ($i = 2, \dots, 5$), it is possible that the peak corresponding to the lighter CP even Higgs might be visible at even lower luminosities. However, for the benchmark points of our choice which are not the most ideal for this purpose as the branching ratio $\chi_2^0 \rightarrow \chi_1^0 H_1$ is not large enough, this possibility can only be realized at very high luminosity options. Using a simple number counting method we observe that with 3000 fb^{-1} luminosity one can achieve a 3σ signal significance to observe the light CP-even Higgs boson (H_1) for our representative benchmark point P3 with stop mass around 1 TeV. The possibility of having significant BR for the decay of $\chi_{2,3}^0$ to both the Higgses ($H_{1,\text{SM}}$) is beyond the scope of this paper, and we try to report this possibility elsewhere [73].

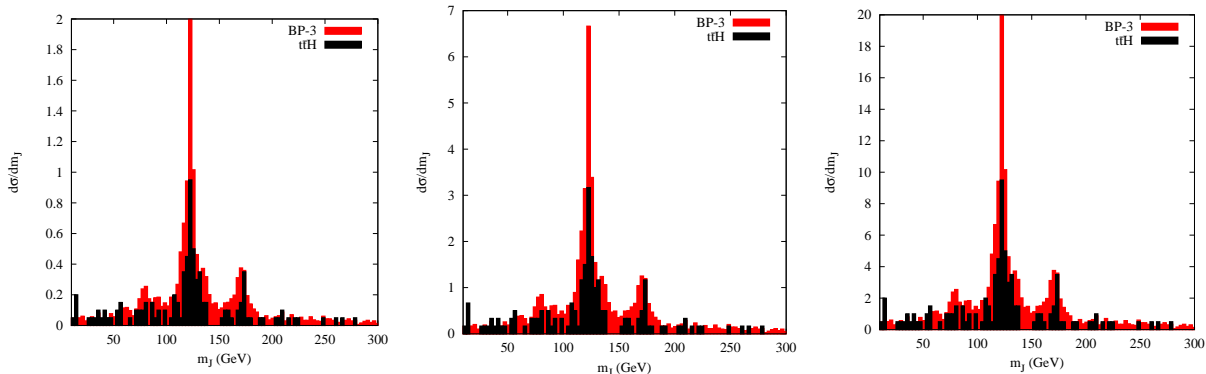


Figure 5: Fat-jet mass distribution with 300 (left), 1000 (middle), 3000 (right) fb^{-1} luminosity, after all cuts as described by the jet substructure analysis in the text. Here we plot first six PT-ordered fat-jet masses at the end of our selection cut (C5), no extra b-tagging criteria on these fat-jets are imposed except the SM Higgs like fat-jets where we demand two b-tagged jets inside the fat-jet. The reason behind this plot is to investigate the possibility of having multiple Higgs peaks in the fat-jet mass distributions. The figures are all normalized to cross section with a particular choice of luminosity.

5 Summary

In this article, we studied Higgs signatures from the cascade decay of the light stop (\tilde{t}_1) in the framework of NMSSM. We identify regions of parameter space where this channel is dominant and consistent with current Higgs coupling measurements, LHC constraints, dark matter relic density and direct detection constraints, and provide a detailed collider simulation of the signal and background. We probe this channel using the jet substructure techniques and via the conventional leptonic searches. It is concluded that in terms of signal to background ratio, the di-lepton channel is the most promising one. In the di-lepton channel we can discover stop masses up to 1.2 TeV with 300 fb^{-1} luminosity. With the jet substructure method, stop masses up to 1 TeV could be probed with 300 fb^{-1} luminosity. Finally we also investigate the possibility of the appearance of multiple Higgs peaks in the fat-jet mass distribution. This is plagued by the low branching ratio to the lighter CP even state in our case, and is only visible at very high luminosity run of the LHC.

6 Acknowledgements

AC would like to thank the Department of Atomic Energy, Government of India for financial support. The work of SM was partially supported by funding available from the Department of Atomic Energy, Government of India, for the Regional Centre for Accelerator-based Particle Physics (RECAPP), Harish-Chandra Research Institute. DS acknowledges Sabine Kraml for a careful reading and valuable suggestions for the manuscript. DS and AC also acknowledges the help of Benjamin Fuks for his help with issues related to NMSSMTools. The work of DS is supported by the French ANR project DM-AstroLHC. DS also acknowledges the hospitality of the Indian Association for the Cultivation of Sciences, Kolkata, where part of the work was completed.

References

- [1] **ATLAS Collaboration** Collaboration, G. Aad *et al.*, “Observation of a new particle in the search for the Standard Model Higgs boson with the ATLAS detector at the LHC,” *Phys.Lett. B716* (2012) 1–29, [arXiv:1207.7214 \[hep-ex\]](https://arxiv.org/abs/1207.7214).
- [2] **CMS Collaboration** Collaboration, S. Chatrchyan *et al.*, “Observation of a new boson at a mass of 125 GeV with the CMS experiment at the LHC,” *Phys.Lett. B716* (2012) 30–61, [arXiv:1207.7235 \[hep-ex\]](https://arxiv.org/abs/1207.7235).
- [3] **ATLAS Collaboration**, G. Aad *et al.*, “Measurement of the Higgs boson mass from the $H \rightarrow \gamma\gamma$ and $H \rightarrow ZZ^* \rightarrow 4\ell$ channels with the ATLAS detector using 25 fb^{-1} of pp collision data,” *Phys.Rev. D90* no. 5, (2014) 052004, [arXiv:1406.3827 \[hep-ex\]](https://arxiv.org/abs/1406.3827).
- [4] **CMS Collaboration**, V. Khachatryan *et al.*, “Precise determination of the mass of the Higgs boson and tests of compatibility of its couplings with the standard model predictions using proton collisions at 7 and 8 TeV,” [arXiv:1412.8662 \[hep-ex\]](https://arxiv.org/abs/1412.8662).
- [5] H. P. Nilles, “Supersymmetry, Supergravity and Particle Physics,” *Phys.Rept.* **110** (1984) 1–162.
- [6] H. E. Haber and G. L. Kane, “The Search for Supersymmetry: Probing Physics Beyond the Standard Model,” *Phys.Rept.* **117** (1985) 75–263.
- [7] S. P. Martin, “A Supersymmetry primer,” *Adv.Ser.Direct.High Energy Phys.* **21** (2010) 1–153, [arXiv:hep-ph/9709356 \[hep-ph\]](https://arxiv.org/abs/hep-ph/9709356).
- [8] M. Papucci, J. T. Ruderman, and A. Weiler, “Natural SUSY Endures,” *JHEP* **1209** (2012) 035, [arXiv:1110.6926 \[hep-ph\]](https://arxiv.org/abs/1110.6926).
- [9] U. Ellwanger, C. Hugonie, and A. M. Teixeira, “The Next-to-Minimal Supersymmetric Standard Model,” *Phys.Rept.* **496** (2010) 1–77, [arXiv:0910.1785 \[hep-ph\]](https://arxiv.org/abs/0910.1785).

[10] M. Bastero-Gil, C. Hugonie, S. King, D. Roy, and S. Vempati, “Does LEP prefer the NMSSM?,” *Phys.Lett.* **B489** (2000) 359–366, [arXiv:hep-ph/0006198 \[hep-ph\]](https://arxiv.org/abs/hep-ph/0006198).

[11] S. King, M. Muhlleitner, and R. Nevzorov, “NMSSM Higgs Benchmarks Near 125 GeV,” *Nucl.Phys.* **B860** (2012) 207–244, [arXiv:1201.2671 \[hep-ph\]](https://arxiv.org/abs/1201.2671).

[12] R. Dermisek and J. F. Gunion, “Escaping the large fine tuning and little hierarchy problems in the next to minimal supersymmetric model and $h \rightarrow aa$ decays,” *Phys.Rev.Lett.* **95** (2005) 041801, [arXiv:hep-ph/0502105 \[hep-ph\]](https://arxiv.org/abs/hep-ph/0502105).

[13] U. Ellwanger, G. Espitalier-Noel, and C. Hugonie, “Naturalness and Fine Tuning in the NMSSM: Implications of Early LHC Results,” *JHEP* **1109** (2011) 105, [arXiv:1107.2472 \[hep-ph\]](https://arxiv.org/abs/1107.2472).

[14] G. G. Ross and K. Schmidt-Hoberg, “The Fine-Tuning of the Generalised NMSSM,” *Nucl.Phys.* **B862** (2012) 710–719, [arXiv:1108.1284 \[hep-ph\]](https://arxiv.org/abs/1108.1284).

[15] G. G. Ross, K. Schmidt-Hoberg, and F. Staub, “The Generalised NMSSM at One Loop: Fine Tuning and Phenomenology,” *JHEP* **1208** (2012) 074, [arXiv:1205.1509 \[hep-ph\]](https://arxiv.org/abs/1205.1509).

[16] G. Belanger, U. Ellwanger, J. F. Gunion, Y. Jiang, S. Kraml, *et al.*, “Higgs Bosons at 98 and 125 GeV at LEP and the LHC,” *JHEP* **1301** (2013) 069, [arXiv:1210.1976 \[hep-ph\]](https://arxiv.org/abs/1210.1976).

[17] U. Ellwanger, “Higgs pair production in the NMSSM at the LHC,” *JHEP* **1308** (2013) 077, [arXiv:1306.5541](https://arxiv.org/abs/1306.5541).

[18] R. Barbieri, D. Buttazzo, K. Kannike, F. Sala, and A. Tesi, “One or more Higgs bosons?,” *Phys.Rev.* **D88** (2013) 055011, [arXiv:1307.4937 \[hep-ph\]](https://arxiv.org/abs/1307.4937).

[19] D. G. Cerdeno, P. Ghosh, and C. B. Park, “Probing the two light Higgs scenario in the NMSSM with a low-mass pseudoscalar,” *JHEP* **1306** (2013) 031, [arXiv:1301.1325 \[hep-ph\]](https://arxiv.org/abs/1301.1325).

[20] Z. Kang, J. Li, T. Li, D. Liu, and J. Shu, “Probing the CP-even Higgs sector via $H_3 \rightarrow H_2 H_1$ in the natural next-to-minimal supersymmetric standard model,” *Phys.Rev.* **D88** no. 1, (2013) 015006, [arXiv:1301.0453 \[hep-ph\]](https://arxiv.org/abs/1301.0453).

[21] M. Badziak, M. Olechowski, and S. Pokorski, “New Regions in the NMSSM with a 125 GeV Higgs,” *JHEP* **1306** (2013) 043, [arXiv:1304.5437 \[hep-ph\]](https://arxiv.org/abs/1304.5437).

[22] F. Franke and H. Fraas, “Production and decay of neutralinos in the next-to-minimal supersymmetric standard model,” *Z.Phys.* **C72** (1996) 309–325, [arXiv:hep-ph/9511275 \[hep-ph\]](https://arxiv.org/abs/hep-ph/9511275).

[23] U. Ellwanger and C. Hugonie, “Neutralino cascades in the (M+1)SSM,” *Eur.Phys.J.* **C5** (1998) 723–737, [arXiv:hep-ph/9712300 \[hep-ph\]](https://arxiv.org/abs/hep-ph/9712300).

[24] S. Choi, D. Miller, and P. Zerwas, “The Neutralino sector of the next-to-minimal supersymmetric standard model,” *Nucl.Phys.* **B711** (2005) 83–111, [arXiv:hep-ph/0407209 \[hep-ph\]](https://arxiv.org/abs/hep-ph/0407209).

[25] K. Cheung and T.-J. Hou, “Light Pseudoscalar Higgs boson in Neutralino Decays in the Next-to-Minimal Supersymmetric Standard Model,” *Phys.Lett.* **B674** (2009) 54–58, [arXiv:0809.1122 \[hep-ph\]](https://arxiv.org/abs/0809.1122).

[26] O. Stal and G. Weiglein, “Light NMSSM Higgs bosons in SUSY cascade decays at the LHC,” *JHEP* **1201** (2012) 071, [arXiv:1108.0595 \[hep-ph\]](https://arxiv.org/abs/1108.0595).

[27] D. Das, U. Ellwanger, and A. M. Teixeira, “Modified Signals for Supersymmetry in the NMSSM with a Singlino-like LSP,” *JHEP* **1204** (2012) 067, [arXiv:1202.5244 \[hep-ph\]](https://arxiv.org/abs/1202.5244).

[28] D. G. Cerdeno, P. Ghosh, C. B. Park, and M. Peir, “Collider signatures of a light NMSSM pseudoscalar in neutralino decays in the light of LHC results,” *JHEP* **1402** (2014) 048, [arXiv:1307.7601 \[hep-ph\]](https://arxiv.org/abs/1307.7601).

[29] U. Ellwanger and A. M. Teixeira, “Excessive Higgs pair production with little MET from squarks and gluinos in the NMSSM,” [arXiv:1412.6394 \[hep-ph\]](https://arxiv.org/abs/1412.6394).

[30] R. Bernabei, P. Belli, F. Cappella, R. Cerulli, C. Dai, A. dAngelo, H. He, A. Incicchitti, H. Kuang, X. Ma, F. Montecchia, F. Nozzoli, D. Prosperi, X. Sheng, R. Wang, and Z. Ye, “New results from dama/libra,” *The European Physical Journal C* **67** no. 1-2, (2010) 39–49. <http://dx.doi.org/10.1140/epjc/s10052-010-1303-9>.

[31] C. E. Aalseth and e. a. Barbeau, “Results from a search for light-mass dark matter with a p -type point contact germanium detector,” *Phys. Rev. Lett.* **106** (Mar, 2011) 131301. <http://link.aps.org/doi/10.1103/PhysRevLett.106.131301>.

[32] **CMS Collaboration** Collaboration, S. Chatrchyan *et al.*, “Search for top-squark pair production in the single-lepton final state in pp collisions at $\sqrt{s} = 8$ TeV,” *Eur.Phys.J.* **C73** no. 12, (2013) 2677, [arXiv:1308.1586 \[hep-ex\]](https://arxiv.org/abs/1308.1586).

[33] **CMS Collaboration** Collaboration, V. Khachatryan *et al.*, “Search for top-squark pairs decaying into Higgs or Z bosons in pp collisions at $\sqrt{s}=8$ TeV,” *Phys.Lett. B* **736** (2014) 371–397, [arXiv:1405.3886 \[hep-ex\]](https://arxiv.org/abs/1405.3886).

[34] **CMS Collaboration** Collaboration, S. Chatrchyan *et al.*, “Search for top squark and higgsino production using diphoton Higgs boson decays,” *Phys.Rev.Lett.* **112** (2014) 161802, [arXiv:1312.3310 \[hep-ex\]](https://arxiv.org/abs/1312.3310).

[35] **ATLAS Collaboration**, G. Aad *et al.*, “Search for direct pair production of a chargino and a neutralino decaying to the 125 GeV Higgs boson in $\sqrt{s} = 8$ TeV pp collisions with the ATLAS detector,” [arXiv:1501.07110 \[hep-ex\]](https://arxiv.org/abs/1501.07110).

[36] D. Ghosh, M. Guchait, and D. Sengupta, “Higgs Signal in Chargino-Neutralino Production at the LHC,” *Eur.Phys.J.* **C72** (2012) 2141, [arXiv:1202.4937 \[hep-ph\]](https://arxiv.org/abs/1202.4937).

[37] D. Ghosh, “Boosted dibosons from mixed heavy top squarks,” *Phys.Rev. D* **88** no. 11, (2013) 115013, [arXiv:1308.0320 \[hep-ph\]](https://arxiv.org/abs/1308.0320).

[38] U. Ellwanger and A. M. Teixeira, “NMSSM with a singlino LSP: possible challenges for searches for supersymmetry at the LHC,” *JHEP* **1410** (2014) 113, [arXiv:1406.7221 \[hep-ph\]](https://arxiv.org/abs/1406.7221).

[39] B. Dutta, Y. Gao, and B. Shakya, “Light Higgsino Decays as a Probe of the NMSSM,” [arXiv:1412.2774 \[hep-ph\]](https://arxiv.org/abs/1412.2774).

[40] U. Ellwanger and C. Hugonie, “NMHDECAY 2.0: An Updated program for sparticle masses, Higgs masses, couplings and decay widths in the NMSSM,” *Comput.Phys.Commun.* **175** (2006) 290–303, [arXiv:hep-ph/0508022 \[hep-ph\]](https://arxiv.org/abs/hep-ph/0508022).

[41] A. Chakraborty, D. K. Ghosh, D. Ghosh, and D. Sengupta, “Stop and sbottom search using dileptonic M_{T2} variable and boosted top technique at the LHC,” *JHEP* **1310** (2013) 122, [arXiv:1303.5776 \[hep-ph\]](https://arxiv.org/abs/1303.5776).

[42] **Particle Data Group** Collaboration, J. Beringer *et al.*, “Review of Particle Physics (RPP),” *Phys.Rev. D* **86** (2012) 010001.

[43] **WMAP** Collaboration, G. Hinshaw *et al.*, “Nine-Year Wilkinson Microwave Anisotropy Probe (WMAP) Observations: Cosmological Parameter Results,” *Astrophys.J.Suppl.* **208** (2013) 19, [arXiv:1212.5226 \[astro-ph.CO\]](https://arxiv.org/abs/1212.5226).

[44] **Planck** Collaboration, P. Ade *et al.*, “Planck 2013 results. XVI. Cosmological parameters,” *Astron.Astrophys.* **571** (2014) A16, [arXiv:1303.5076 \[astro-ph.CO\]](https://arxiv.org/abs/1303.5076).

[45] **LUX Collaboration** Collaboration, D. Akerib *et al.*, “First results from the LUX dark matter experiment at the Sanford Underground Research Facility,” *Phys. Rev. Lett.* **112** (2014) 091303, [arXiv:1310.8214 \[astro-ph.CO\]](https://arxiv.org/abs/1310.8214).

[46] G. Degrassi, S. Heinemeyer, W. Hollik, P. Slavich, and G. Weiglein, “Towards high precision predictions for the MSSM Higgs sector,” *Eur. Phys. J. C* **28** (2003) 133–143, [arXiv:hep-ph/0212020 \[hep-ph\]](https://arxiv.org/abs/hep-ph/0212020).

[47] M. D. Goodsell, K. Nickel, and F. Staub, “Two-loop corrections to the Higgs masses in the NMSSM,” *Phys. Rev. D* **91** no. 3, (2015) 035021, [arXiv:1411.4665 \[hep-ph\]](https://arxiv.org/abs/1411.4665).

[48] **ATLAS** Collaboration, G. Aad *et al.*, “Measurement of Higgs boson production in the diphoton decay channel in pp collisions at center-of-mass energies of 7 and 8 TeV with the ATLAS detector,” *Phys. Rev. D* **90** no. 11, (2014) 112015, [arXiv:1408.7084 \[hep-ex\]](https://arxiv.org/abs/1408.7084).

[49] **ATLAS** Collaboration, G. Aad *et al.*, “Observation and measurement of Higgs boson decays to WW^* with the ATLAS detector,” [arXiv:1412.2641 \[hep-ex\]](https://arxiv.org/abs/1412.2641).

[50] **ATLAS** Collaboration, G. Aad *et al.*, “Measurements of Higgs boson production and couplings in the four-lepton channel in pp collisions at center-of-mass energies of 7 and 8 TeV with the ATLAS detector,” *Phys. Rev. D* **91** no. 1, (2015) 012006, [arXiv:1408.5191 \[hep-ex\]](https://arxiv.org/abs/1408.5191).

[51] **ATLAS** Collaboration, G. Aad *et al.*, “Search for the $b\bar{b}$ decay of the Standard Model Higgs boson in associated $(W/Z)H$ production with the ATLAS detector,” *JHEP* **1501** (2015) 069, [arXiv:1409.6212 \[hep-ex\]](https://arxiv.org/abs/1409.6212).

[52] **ATLAS** Collaboration, G. Aad *et al.*, “Evidence for the Higgs-boson Yukawa coupling to tau leptons with the ATLAS detector,” [arXiv:1501.04943 \[hep-ex\]](https://arxiv.org/abs/1501.04943).

[53] **Heavy Flavor Averaging Group (HFAG)** Collaboration, Y. Amhis *et al.*, “Averages of b -hadron, c -hadron, and τ -lepton properties as of summer 2014,” [arXiv:1412.7515 \[hep-ex\]](https://arxiv.org/abs/1412.7515).

[54] J. M. Butterworth, A. R. Davison, M. Rubin, and G. P. Salam, “Jet substructure as a new Higgs search channel at the LHC,” *Phys. Rev. Lett.* **100** (2008) 242001, [arXiv:0802.2470 \[hep-ph\]](https://arxiv.org/abs/0802.2470).

[55] Y. L. Dokshitzer, G. Leder, S. Moretti, and B. Webber, “Better jet clustering algorithms,” *JHEP* **9708** (1997) 001, [arXiv:hep-ph/9707323 \[hep-ph\]](https://arxiv.org/abs/hep-ph/9707323).

[56] U. Ellwanger and C. Hugonie, “NMSPEC: A Fortran code for the sparticle and Higgs masses in the NMSSM with GUT scale boundary conditions,” *Comput. Phys. Commun.* **177** (2007) 399–407, [arXiv:hep-ph/0612134 \[hep-ph\]](https://arxiv.org/abs/hep-ph/0612134).

[57] U. Ellwanger, J. F. Gunion, and C. Hugonie, “NMHDECAY: A Fortran code for the Higgs masses, couplings and decay widths in the NMSSM,” *JHEP* **0502** (2005) 066, [arXiv:hep-ph/0406215 \[hep-ph\]](https://arxiv.org/abs/hep-ph/0406215).

[58] D. Das, U. Ellwanger, and A. M. Teixeira, “NMSDECAY: A Fortran Code for Supersymmetric Particle Decays in the Next-to-Minimal Supersymmetric Standard Model,” *Comput. Phys. Commun.* **183** (2012) 774–779, [arXiv:1106.5633 \[hep-ph\]](https://arxiv.org/abs/1106.5633).

[59] J. Alwall, M. Herquet, F. Maltoni, O. Mattelaer, and T. Stelzer, “MadGraph 5 : Going Beyond,” *JHEP* **1106** (2011) 128, [arXiv:1106.0522 \[hep-ph\]](https://arxiv.org/abs/1106.0522).

[60] T. Sjostrand, S. Mrenna, and P. Z. Skands, “PYTHIA 6.4 Physics and Manual,” *JHEP* **0605** (2006) 026, [arXiv:hep-ph/0603175 \[hep-ph\]](https://arxiv.org/abs/hep-ph/0603175).

[61] S. Hoeche, F. Krauss, N. Lavesson, L. Lonnblad, M. Mangano, *et al.*, “Matching parton showers and matrix elements,” [arXiv:hep-ph/0602031 \[hep-ph\]](https://arxiv.org/abs/hep-ph/0602031).

[62] M. Cacciari, G. P. Salam, and G. Soyez, “FastJet User Manual,” *Eur.Phys.J. C72* (2012) 1896, [arXiv:1111.6097 \[hep-ph\]](https://arxiv.org/abs/1111.6097).

[63] M. Cacciari, G. P. Salam, and G. Soyez, “The Anti-k(t) jet clustering algorithm,” *JHEP 0804* (2008) 063, [arXiv:0802.1189 \[hep-ph\]](https://arxiv.org/abs/0802.1189).

[64] “Calibration of the performance of b -tagging for c and light-flavour jets in the 2012 ATLAS data.”.

[65] C. Lester and D. Summers, “Measuring masses of semiinvisibly decaying particles pair produced at hadron colliders,” *Phys.Lett. B463* (1999) 99–103, [arXiv:hep-ph/9906349 \[hep-ph\]](https://arxiv.org/abs/hep-ph/9906349).

[66] A. Barr, C. Lester, and P. Stephens, “m(T2): The Truth behind the glamour,” *J.Phys. G29* (2003) 2343–2363, [arXiv:hep-ph/0304226 \[hep-ph\]](https://arxiv.org/abs/hep-ph/0304226).

[67] A. J. Barr and C. Gwenlan, “The Race for supersymmetry: Using m(T2) for discovery,” *Phys.Rev. D80* (2009) 074007, [arXiv:0907.2713 \[hep-ph\]](https://arxiv.org/abs/0907.2713).

[68] T. Plehn, M. Spannowsky, M. Takeuchi, and D. Zerwas, “Stop Reconstruction with Tagged Tops,” *JHEP 1010* (2010) 078, [arXiv:1006.2833 \[hep-ph\]](https://arxiv.org/abs/1006.2833).

[69] T. Plehn, M. Spannowsky, and M. Takeuchi, “Stop searches in 2012,” *JHEP 1208* (2012) 091, [arXiv:1205.2696 \[hep-ph\]](https://arxiv.org/abs/1205.2696).

[70] G. Belanger, D. Ghosh, R. Godbole, M. Guchait, and D. Sengupta, “Probing the flavor violating scalar top quark signal at the LHC,” *Phys.Rev. D89* (2014) 015003, [arXiv:1308.6484 \[hep-ph\]](https://arxiv.org/abs/1308.6484).

[71] C. Borschensky, M. Krmer, A. Kulesza, M. Mangano, S. Padhi, *et al.*, “Squark and gluino production cross sections in pp collisions at $\sqrt{s} = 13, 14, 33$ and 100 TeV,” *Eur.Phys.J. C74* no. 12, (2014) 3174, [arXiv:1407.5066 \[hep-ph\]](https://arxiv.org/abs/1407.5066).

[72] “LHC Higgs working group ,”.
<https://twiki.cern.ch/twiki/bin/view/LHCPhysics/CERNYellowReportPageAt1314TeV>.

[73] A. Chakraborty, D. K. Ghosh, S. Mondal, S. Poddar, and D. Sengupta, “Multiple Higgs peak in the NMSSM (in preparation),”.